Journal of Molecular Graphics and Modelling 52 (2014) 30–35

Contents lists available at ScienceDirect

Journal of Molecular Graphics and Modelling

journal homepage: www.elsevier.com/locate/JMGM

Trends in predicted chemoselectivity of cytochrome P450 oxidation: B3LYP barrier heights for epoxidation and hydroxylation reactions☆

Patrik Rydberg[a], Richard Lonsdale[b], Jeremy N. Harvey[b], Adrian J. Mulholland[b], Lars Olsen[a,*]

[a] Department of Drug Design and Pharmacology, Faculty of Health and Medical Sciences, University of Copenhagen, Universitetsparken 2, DK-2100 Copenhagen, Denmark
[b] Centre for Computational Chemistry, School of Chemistry, University of Bristol, Cantock's Close, Bristol BS8 1TS, United Kingdom

ARTICLE INFO

Article history:
Accepted 12 June 2014
Available online 23 June 2014

Keywords:
Density functional theory
B3LYP
Dispersion
Aliphatic hydroxylation
Epoxidation

ABSTRACT

Prediction of epoxide formation in drug metabolism is a difficult but important task, as epoxide formation is linked to drug toxicity. A comparison of the energy barriers for cytochrome P450 mediated epoxidation of alkenes to the barriers for the hydroxylation of an aliphatic carbon atom next to a double bond has been performed using B3LYP and B3LYP-D3. Relevant experimental data on oxidation selectivity has also been assessed. The results show that density functional theory, when using B3LYP-D3, does well in reproducing the experimental trends. Considering that the comparison involves chemical steps with quite different features this is remarkable. We also find that B3LYP consistently underestimates the hydrogen abstraction barriers relative to the epoxidation barriers, and that including a dispersion correction reduces this problem.

1. Introduction

The formation of reactive metabolites has been connected to toxicity for numerous drugs [1]. The formation of such metabolites is commonly mediated by cytochromes P450 (CYPs), a family of monooxygenase enzymes that is involved in the metabolism of most drugs [2]. CYPs are capable of mediating a large number of different types of reactions, including hydroxylation of aliphatic and aromatic carbon atoms, epoxidation of double bonds, oxidation of sulphur and nitrogen atoms, and oxidation of aldehydes. One of the most common reactions leading to reactive metabolites is the epoxidation of double bonds. Currently, methods for predicting drug metabolism by CYPs struggle with the prediction of epoxidation of double bonds, due to the fact that the energy barriers for epoxidation, and hydroxylation of an aliphatic carbon next to a double bond are quite similar, leading to a high uncertainty in predictions [3].

During the last decade the density functional theory method B3LYP [4–6] has been used extensively in studies of reaction mechanisms in CYPs [7–9]. Whilst B3LYP has been shown to perform less well than other functionals (such as BP86, PBE, PBE0, TPSS, TPSSH, B3LYP, and B97-D) for the calculation of geometries of iron porphyrin complexes [10], the geometries are sufficiently accurate to provide a satisfactory description of the energetics of such systems [11]. B3LYP is also known to reproduce the relative spin state energies of iron porphyrins [8], and give energies in agreement with CCSD(T) for such systems, e.g. energy barriers for NO and CO binding to heme [12]. Together, these results have led to B3LYP becoming a widely used method in the study of CYP mediated reactions.

B3LYP has been previously shown to give systematic errors related to dispersion interactions [13], isomerization energies and heats of formation [14], as well as for energy barriers for a database dominated by hydrogen-atom-transfer reactions [15]. Friesner et al., in a series of publications [16–18], have shown that errors in B3LYP, with regard to a large number of properties, can be alleviated by the inclusion of empirical parameters in a systematic fashion. Hence, the existence of systematic errors in the results on CYP-mediated reactions cannot be excluded. Recent work has also indicated that B3LYP-calculated barriers to oxidation of propene by Compound I artificially favour hydroxylation relative to epoxidation [19], and that the addition of a dispersion correction improves the relation between B3LYP barriers and experimental data, both when using model systems and QM/MM calculations [20,21].

In this study we have investigated how the relative activation barriers of epoxidation and hydroxylation reactions performed by cytochromes P450, computed by theoretical methods, relate to experimental product distributions. To achieve this, we have

☆ This manuscript is dedicated to Patrik Rydberg, deceased prior to publication.

* Corresponding author. Tel.: +45 35 33 63 05; fax: +45 35 33 60 41.
E-mail address: lo@sund.ku.dk (L. Olsen).

http://dx.doi.org/10.1016/j.jmgm.2014.06.002
1093-3263/

calculated the transition states (TS) for the step with the highest activation energy for each of the two reaction mechanisms. A set of five diverse substrates has been investigated, so as to expand the conclusions significantly compared to the simple alkenes studied previously [20] using the B3LYP functional, both with and without an empirical dispersion correction (B3LYP-D3 [22]). We observe that the B3LYP predicted balance between epoxidation and hydroxylation reactions is tilted somewhat in favour of hydroxylation compared to what is observed experimentally. Including the dispersion correction decreases this apparent bias, but does not remove it in all cases.

2. Computational methodology

All calculations were performed with the Turbomole software package [23], version 6.3.1. Compound I was modelled as an iron porphine with SCH_3^- and O^{2-} as axial ligands. The B3LYP functional [4–6] with the VWN(V) correlation functional [24] (unrestricted formalism for open shell systems) was used throughout. The geometry optimization and frequency calculations were performed using the double-ζ basis set of Schäfer et al. [25], enhanced with a *p* function with an exponent of 0.134915 on the iron atom, and the 6-31G(d) basis set [26–28] for all other atoms. This basis set combination is referred to as BS1 in the remainder of the text. The final energies were determined by performing single point calculations using the double-ζ basis set of Schäfer et al. [25], enhanced with *s*, *p*, *d*, and *f* functions (exponents of 0.01377232, 0.041843, 0.1244, 2.5, and 0.8; two *f* functions) [29] for iron, and the 6-311++G(2d,2p) basis set [30,31] for all other atoms (referred to herein at BS2). All transition states were verified by performing frequency calculations using BS1, and each was found to have a single imaginary frequency with the normal mode connecting substrate and product.

Despite the relative simplicity of the system, there are multiple conformers of each transition state for each substrate and reaction type, and it is important to locate the lowest energy TS in each case. Therefore, TS optimization was initiated from multiple different structures, in which the orientation of the substrates relative to the porphyrin ring was changed. In order to generate the different starting structures for geometry optimization, it was convenient to start from structures generated in previous work. For the transition states for propene [20], cyclohexene [20], and caffeine [32], previous work on the TSs was available and was used for this purpose. In the case of butadiene monoxide and the quinidine fragment, the propene structures were used as a starting point. Also, different spin states and different methods can return lowest energy TSs that correspond to different conformers. Careful evaluation of the results in order to eliminate inconsistencies of this type was therefore performed.

For direct comparison to previous work, the cyclohexene reactions were also computed using the iron basis sets used previously [20]. These basis sets, which include effective core potentials, are the LANLTZ [33] basis set in BS1 and the SDD [34] basis set in BS2. This combination is called SDD/LANLTZ in the remainder of the text. When describing geometrical features it is only referred to as LANLTZ (as SDD is only used for energy calculations).

A dispersion correction was calculated using the D3-formalism [22] for all reactions, and additionally calculations with D2-formalism [35,36] were performed for the cyclohexene reactions. When calculating dispersion-corrected energies, the dispersion correction was used for all calculations (geometry optimizations, frequency calculations and single point energy calculations).

3. Results and discussion

To investigate the relative barriers of aliphatic hydrogen abstraction reactions, compared to epoxidations and aromatic oxidations, we sought to use a fairly large and diverse set of test compounds. The five compounds used were selected on the basis that experimental data concerning selectivity was available, and also that there was some evidence that the barriers to the two types of reaction were somewhat similar. This evidence could either be experimental (observation of both products during oxidation by cytochrome P450), or computational (prediction of similar energy barriers for similar fragments in previous calculations). The compounds chosen were butadiene monoxide, caffeine, cyclohexene, propene, and a fragment of quinidine (shown in Fig. 1).

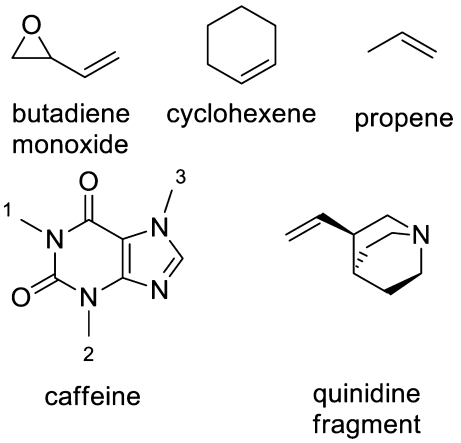

Fig. 1. The five compounds studied, with the three hydroxylation sites on caffeine numbered.

Trends in the experimental data for compounds with double bonds without nearby hetero-atoms (i.e. not butadiene monoxide) show that the amount of hydroxylated product relative to the epoxide is larger for more highly substituted allylic positions, i.e. for carbon atoms adjacent to the double bond bearing fewer hydrogen atoms. Thus the trend for the amount of hydroxylated product is CH (quinidine [45], quinine [44], vitamin D2 [46]) > CH_2(cyclohexene [41,42]) > CH_3(propene [43], 2-butene [43]), which correlates to the radical stability of the intermediate in the hydrogen abstraction mechanism [47].

To investigate how well B3LYP and B3LYP-D3 reproduces these data we computed the epoxidation barriers and hydroxylation barriers for the sites adjacent to the double bonds in the compounds shown in Fig. 1 (experimental data and references for these compounds are shown in Table 1) and the aromatic oxidation and aliphatic hydroxylation barriers for caffeine. For these calculations, we have used a small cluster model [48] of the Compound I species, rather than a detailed atomistic representation of the whole enzyme. This is partly for computational convenience, but also because we have found previously [19–21] that for small substrates with low polarity, like most of those studied here, the effect of the protein environment on relative barriers is small. Additionally, for the comparisons of theoretical and experimental data we have preferred to use data from the 3A4 isoform where available, as this isoform has the largest and most flexible active site [49], thus reducing the effects of interactions between the substrate and the binding site on which metabolites are formed.

Our focus in this study is to examine the relative rate of epoxidation and hydroxylation. This is dependent on the difference in free energy between the corresponding TSs, with the *absolute* activation free energies for each of the two pathways being of less interest. Accordingly, we only present here calculated relative energies and free energies for the transition states, taking the sum of the energies of the separate Compound I and substrate as a reference. We note that this choice of reference appears to return anomalously low 'activation' energies in the case of some of the dispersion-corrected

Table 1
Summary of experimental data relevant for comparison to the calculations of the five compounds studied in this work.

Molecule	Epoxidation/aromatic oxidation	Hydroxylation
Butadiene monoxide [37]	Only metabolite in 2A6, 2C9, and 2E1.	N/A
Caffeine [38,39]	Major metabolite in 3A4 and several other isoforms.	Site 3 is secondary metabolite in 3A4, site 2 third, and site 1 fourth.
Cyclohexene [40–42]	Major metabolite in 2B4, equal in 2E1. Minor in P450cam.	Minor in 2B4, equal in 2E1, major in P450cam.
Propene [43]	Only metabolite in 2B4.	N/A
Quinidine fragment [44,45]	Minor metabolite in quinine in 3A4.	Major metabolite in quinidine and quinine in 3A4.

energy barriers (as has been shown previously [20]). A more careful consideration of the free energy of the resting state of the enzyme would change these anomalously low values, but would have no effect on the relative barriers that we are interested in here.

As the energy barriers calculated for cyclohexene oxidation did not fully agree with other previous results [20], we decided to investigate the epoxidation and hydroxylation of cyclohexene more extensively than the corresponding reactions for the other compounds. Hence, these two reactions were computed with B3LYP, B3LYP-D2, and B3LYP-D3, with two different basis set combinations: the BS2/BS1 combination used for all the other compounds; and secondly, replacing the Schäfer iron basis sets with the SDD/LANLTZ basis set and effective core potential, as used in the previous work [20].

Even for the relative energies of epoxidation and hydroxylation TSs (shown in Table 2), some changes are observed between results depending on the functional used, and the basis set. It is perhaps helpful to start with some general observations. We consider first the difference in energy between quartet and doublet TSs. In the case of the epoxidation reaction, barrier heights relative to separated reactants are somewhat dependent on the basis set used, and especially on the treatment of dispersion (B3LYP vs. B3LYP-D2 and B3LYP-D3). However, the transition state on the doublet surface is consistently slightly lower in energy compared to the quartet spin state (5–8 kJ/mol). In the case of the hydroxylation reaction, things are slightly less simple. The transition state on the quartet potential energy surface is consistently lower in energy when using B3LYP-D3, but the difference with respect to the doublet TS is rather dependent on the basis set and dispersion treatment. For example, with the BS2 basis set, the quartet is 0.5–2.1 kJ/mol lower in energy than for the doublet state, whereas with the SDD/LANTZ basis set the quartet TS is 3.1–5.6 kJ/mol lower than the doublet one. In general, we find that the effect of changing the basis set on relative TS energies is of the order of 3 kJ/mol, when calculations are performed in a consistent manner.

Next, we note that some discrepancies are observed for TS energies between the present and previous work [20]. These can be attributed to several factors. Firstly, slight differences (in the order of 1–2 kJ/mol) are expected when using different QM codes and basis sets (ORCA was used in the previous work, Turbomole in the present work). Next, as discussed above, there are many different possible conformers for the TSs, and it appears that one type of conformeric variability was missed for one TS in the previous work. This is shown by the fact that the most significant discrepancies between the present and previous work (highlighted in bold in Table 2) lay with the doublet epoxidation transition state energies, calculated both with and without dispersion (D2). On comparison between the optimized geometries from the previous and present work, notable differences were observed between these structures, primarily due to rotation of the thiomethyl group bound to the iron atom of the heme. No such differences were noted for the other calculations, where a much better agreement is observed between the present and previous work. The potential energy surfaces of cyclohexene hydroxylation and epoxidation have multiple saddle points that correspond to different local minima on the ridge separating reactants and products. Apparently some of the energies and structures reported for the transition states in the previous work related to local rather than global minima on this ridge. As the structural optimizations performed in the present work were initiated from the structures obtained previously, one might have expected that similar structures – the 'same' local minima – would be obtained. The fact that somewhat different structures are found here suggests that the potential energy surface is relatively flat, with small differences in basis set and optimization method (B3LYP-D3 vs. B3LYP-D2) being sufficient to perturb the optimizations towards other, lower-energy transition states. In the previous work, the B3LYP-D2 barrier to hydroxylation on the quartet spin surface was found to be 6.7 kJ/mol higher than that of the doublet, whereas in the present work the quartet barriers were found to be lower in energy than the doublet, although by a smaller amount. Analysis of the hydroxylation TS structures reveals that the geometries agree well between the previous and current work, with the exception of the quartet hydroxylation TS calculated with B3LYP-D2 in the previous work (the outlier in Table 2). To make sure that the differences in results were not due to the variations in software setup further tests were carried out by performing optimizations on all of the TS geometries calculated in the present work using the methods used in the previous work [20] and a good agreement was found between the two sets of calculations, both in terms of geometries and energies.

The B3LYP-D2 and B3LYP-D3 optimized structures for the epoxidation transition states are much more similar in the quartet spin state than they are in the doublet spin state (see the Fe–O–C angle in Table 3). This is true for both basis set combinations (BS1 and

Table 2
Transition state energies for the calculations of cyclohexene reactions with the various B3LYP and basis set combinations. Vacuum energies in kJ/mol without zero point vibrational energies relative to the separate compound I and cyclohexene. Energies relative to the lowest barrier are in parenthesis. Bold face indicates previously published calculations with significant deviations compared to the data from this study.

	Epoxidation		Hydroxylation	
	Doublet	Quartet	Doublet	Quartet
Previous work [20] B3LYP	**73.2 (7.5)**	68.2 (2.5)	73.2 (7.5)	65.7 (0.0)
Previous work [20] B3LYP-D2	**18.0 (2.1)**	15.9 (0.0)	23.0 (7.1)	**29.7 (13.8)**
B3LYP BS2/BS1	57.8 (0.0)	65.1 (7.3)	66.7 (8.9)	64.6 (6.8)
B3LYP SDD/LANLTZ	59.0 (0.0)	64.5 (5.5)	69.3 (10.3)	63.7 (4.7)
B3LYP-D2 BS2/BS1	2.7 (0.0)	10.9 (8.2)	21.6 (18.9)	20.0 (17.3)
B3LYP-D2 SDD/LANLTZ	4.4 (0.0)	10.1 (5.7)	23.6 (19.2)	19.2 (14.7)
B3LYP-D3 BS2/BS1	6.6 (0.0)	15.0 (8.4)	24.8 (18.2)	24.3 (17.7)
B3LYP-D3 SDD/LANLTZ	7.8 (0.0)	14.7 (6.9)	26.7 (19.0)	23.7 (15.9)

Table 3
Comparison of key properties for the transition state geometries for the epoxidation of cyclohexene calculated with the various B3LYP and basis set combinations.

Method	BS1		LANLTZ	
	Doublet	Quartet	Doublet	Quartet
		Fe—S (Å)		
B3LYP	2.345	2.360	2.363	2.375
B3LYP-D2	2.327	2.329	2.342	2.342
B3LYP-D3	2.326	2.326	2.338	2.340
		Fe—O (Å)		
B3LYP	1.720	1.732	1.708	1.721
B3LYP-D2	1.713	1.726	1.702	1.713
B3LYP-D3	1.711	1.731	1.699	1.718
		O—C (Å)		
B3LYP	2.142	1.984	2.146	1.960
B3LYP-D2	2.221	2.029	2.160	2.012
B3LYP-D3	2.212	1.991	2.243	1.968
		Fe—O—C (degrees)		
B3LYP	127.55	133.65	128.36	134.25
B3LYP-D2	117.27	133.42	127.65	132.58
B3LYP-D3	123.96	135.30	124.24	134.86

LANLTZ). The inclusion of dispersion also affects the structures calculated in the doublet spin state much more than it does those obtained for the quartet spin state. As was shown in previous work [20], the dispersion correction leads to orientations in which the cyclohexene is positioned slightly closer to the heme in epoxidation transition states (see Fig. 2). With the exception of the transition state to epoxidation calculated in the doublet spin state with B3LYP-D2, the geometries for the two basis set combinations (BS1 and LANLTZ) are quite similar. The observed difference in geometry for the doublet spin state with B3LYP-D2 is similar to what was found for the transition state for the sulfoxidation of dimethylsulfide in the doublet spin state [50], and is probably caused by a very flat potential energy surface (calculations using BS2 and D2 dispersion on the D3 structure and the opposite gives energy differences of only 2 kJ/mol).

As in previous work [20], two different geometries are found for the hydrogen abstraction transition states, one where cyclohexene is in a vertical position and one where it is parallel to the heme group (see Fig. 3). The vertical structure is preferred in the B3LYP calculations, whereas the parallel structure is preferred in the B3LYP-D2 and B3LYP-D3 calculations. However, the energy differences between the two structures are not very large (5.7 and 6.5 kJ/mol for B3LYP in the doublet and quartet spin states, respectively, and 3.0 and 2.4 kJ/mol for B3LYP-D3 in the doublet and quartet spin states, respectively), and thus, interactions with the active site in a protein can most likely change the preference

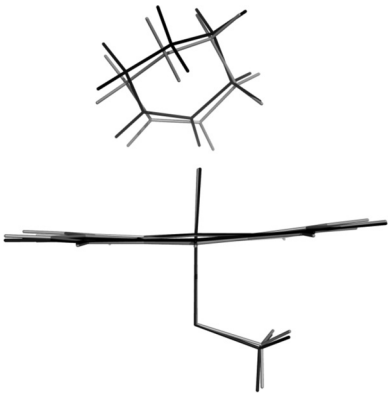

Fig. 2. Comparison of non-dispersion and dispersion corrected structures of the transition state for the epoxidation of cyclohexene computed using B3LYP (black) and B3LYP-D3 (grey) with the BS2/BS1 basis set combination in the doublet spin state.

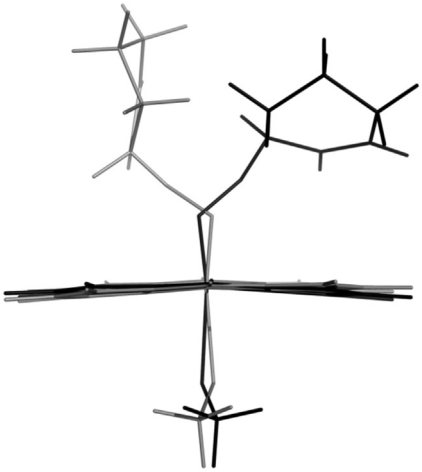

Fig. 3. Comparison of the parallel (black) and upright (grey) structures of the transition state for the hydroxylation of cyclohexene computed using B3LYP with the BS2/BS1 basis set combination in the doublet spin state.

between the two variants. For both the parallel and vertical structures, we find that B3LYP-D2 tends to favour structures with a slightly shorter distance between the cyclohexene and the heme compared to B3LYP-D3, which can also be seen in the Fe–O–H angle in Table 4.

Summaries of the calculations on the remaining four substrates together with cyclohexene are shown in Table 5 (spin-state specific energies are available in the supporting information). Additional details and structures are available in the supporting information.

When considering the individual substrates in Table 5, the best agreement between the calculated relative energies and experiment is observed for caffeine, for which all four of the method combinations predict the correct experimental ordering of preference for oxidation at all four sites. Whilst butadiene monoxide and propene oxidations are predicted correctly by three out of the four

Table 4
Comparison of key properties for the transition state geometries for the hydroxylation of cyclohexene calculated with the various B3LYP and basis set combinations. The data is taken from the structure (parallel or upright, see Fig. 3) with the lowest energy for each combination.

Method	BS1		LANLTZ	
	Doublet	Quartet	Doublet	Quartet
		Fe—S (Å)		
B3LYP	2.325	2.360	2.346	2.381
B3LYP-D2	2.312	2.338	2.357	2.354
B3LYP-D3	2.318	2.336	2.354	2.352
		Fe—O (Å)		
B3LYP	1.734	1.730	1.718	1.719
B3LYP-D2	1.725	1.729	1.696	1.718
B3LYP-D3	1.724	1.732	1.701	1.720
		O—H (Å)		
B3LYP	1.385	1.285	1.404	1.276
B3LYP-D2	1.419	1.293	1.402	1.283
B3LYP-D3	1.399	1.286	1.399	1.277
		H—C (Å)		
B3LYP	1.207	1.284	1.202	1.294
B3LYP-D2	1.189	1.271	1.204	1.281
B3LYP-D3	1.199	1.282	1.205	1.293
		Fe—O—H (degrees)		
B3LYP	118.01	123.85	119.20	124.12
B3LYP-D2	115.74	121.37	118.52	121.83
B3LYP-D3	117.90	123.28	120.10	123.78
		O—H—C (degrees)		
B3LYP	167.109	167.44	167.77	168.22
B3LYP-D2	163.113	165.80	167.33	166.74
B3LYP-D3	162.33	164.92	165.78	165.97

Table 5
Energy barriers with zero-point energy correction for the five compounds with B3LYP and B3LYP-D3 using the BS2/BS1 basis sets in kJ/mol relative to the separate compound I and substrate (energies without zero-point energy correction in parenthesis). Energies are only shown for the spin state that results in the lowest energy. Bold face marks sites which are correctly ordered by energy compared to the experimental data shown in Table 1.

Molecule	B3LYP		B3LYP-D3	
	Epoxidation or aromatic oxidation	Hydroxylation	Epoxidation or aromatic oxidation	Hydroxylation
Butadiene monoxide	61.8 (**60.0**)	59.2 (74.7)	**19.7 (16.3)**	21.7 (35.1)
Caffeine[a]	**50.2 (50.2)**	**62.3/57.0/51.7 (77.1/71.3/65.7)**	**−12.4 (−13.8)**	**14.3/9.0/3.7 (26.8/20.7/16.1)**
Cyclohexene[b]	58.9 (57.8)	50.4 (64.6)	**9.1** (6.6)	**11.3** (24.3)
Propene	63.4 (**61.4**)	56.6 (69.4)	**22.5 (20.0)**	23.5 (35.2)
Quinidine fragment	62.1 (60.3)	**48.3** (62.5)	8.4 (5.6)	**−7.6 (5.1)**

[a] The three hydroxylation sites shown in Fig. 1 are ordered consecutively and separated by '/'.
[b] The cyclohexene sites are bold faced when the difference of epoxidation and hydroxylation is less than 3.4 kJ/mol. This corresponds to a change in product distribution from 1:2 to 2:1, which is the variation found in Refs. [40–42].

methods (only B3LYP with zero-point energy correction incorrectly predicts hydroxylation for both substrates), the energy difference is smaller than expected for B3LYP-D3 with zero-point energy corrections. For the quinidine fragment, the hydroxylation reaction is correctly predicted to have a lower barrier than the epoxidation reaction by all methods except for B3LYP without zero-point energy corrections. However, considering that the hydroxylated quinidine species is not the only observed product (a small amount of epoxide is formed), the energy difference is probably too large for both B3LYP and B3LYP-D3 when including zero-point energy corrections. Cyclohexene is more difficult to interpret, as we know from experiments that the amount of epoxide relative to the hydroxylated product can vary from major to minor product depending in the CYP isoform involved (Table 1) [40–42]. The relative amounts of epoxide and hydroxylated products vary from 1:2 to 2:1 among the different CYP isoforms tested, which corresponds to a free energy difference of 3.4 kJ/mol. Assuming that the perturbation by the enzyme binding site on the energy barrier is less than this, the only method that can correctly predict the product formed is B3LYP-D3 with zero-point energy corrections (with an energy difference of 2.2 kJ/mol).

Taking all of the B3LYP results into account (in the absence of dispersion), it seems clear that including zero-point energy corrections results in too large a preference for aliphatic hydroxylations (especially since tunnelling effects have not been included in this study – which would further favour hydroxylation), whereas excluding zero-point energy corrections gives too much preference for epoxidations. An earlier study by Hughes et al. suggested that hydrogen abstraction barriers in CYPs computed by B3LYP are severely overestimated [51]. If this is true, then our results show that the epoxidation barriers are overestimated to an even greater extent.

Still, considering that the two reaction types that we are studying have very different chemical features, it is clear that B3LYP-D3 is quite good at reproducing the experimental trends when including zero-point energy corrections. Nevertheless, it appears that some errors remain even when using this approach. For future calculations, we recommend the usage of B3LYP-D3 with zero-point energy corrections for comparative studies of epoxidation and hydroxylations in cytochromes P450.

4. Conclusions

The relation between experimental product distributions and the relative transition state energies for hydroxylation reactions and epoxidation/aromatic oxidation reactions performed by cytochrome P450 enzymes has been investigated for five diverse substrates, using a model system and density functional theory with the B3LYP functional with and without dispersion correction.

The results show clearly that B3LYP tends to underestimate the barriers for hydroxylation relative to epoxidation, and considering that earlier work suggests that the absolute hydroxylation barriers are overestimated [51] this indicates that the epoxidation barriers are even more overestimated.

A dispersion correction in the form of B3LYP-D3 with additional zero point energy corrections was found to give significant improvements in the relative barrier heights, and successfully predicts the major experimentally observed metabolite as that with the lowest barrier for all of our test compounds. As the substrates studied are relatively small and mostly non-polar, effects from the protein environment on the relative barrier height for the two reactions should be small, so that even though our calculations use a cluster model, the results should be comparable to experimental outcomes in the enzymes. Thus, for future studies of CYP-mediated reactions, especially when comparing mechanisms with different chemical features, the use of B3LYP-D3 is recommended.

Additionally, two different basis sets were compared for the hydroxylation and epoxidation of cyclohexene. For the two different basis sets used, one all-electron basis set and one with an effective core potential, both give similar geometries and transition state energies.

Supporting information

Electronic Supplementary Information (ESI) available: Structures in *xyz* format for all computed complexes, energies for all complexes and spin states.

Acknowledgements

PR thanks Lhasa Limited for support. AJM and RL thank EPSRC for support under the CCP-BioSim project (grant number: EP/J010588/1; www.ccpbiosim.ac.uk). AJM is an EPSRC leadership fellow (grant number: EP/G007705/01) and together with RL and JNH thanks EPSRC for support. JNH holds a Royal Society Wolfson Research Merit Award.

Appendix A. Supplementary data

Supplementary data associated with this article can be found, in the online version, at http://dx.doi.org/10.1016/j.jmgm.2014.06.002.

References

[1] R.A. Thompson, E.M. Isin, Y. Li, R. Weaver, L. Weidolf, I. Wilson, A. Claesson, K. Page, H. Dolgos, J.G. Kenna, Risk assessment and mitigation strategies for reactive metabolites in drug discovery and development, Chem. Biol. Interact. 192 (2011) 65–71, http://dx.doi.org/10.1016/j.cbi.2010.11.002.

[2] F.P. Guengerich, Cytochrome P450s and other enzymes in drug metabolism and toxicity, AAPS J. 8 (2006) E101–E111, http://dx.doi.org/10.1208/aapsj080112.
[3] P. Rydberg, L. Olsen, Predicting drug metabolism by cytochrome P450 2C9: comparison with the 2D6 and 3A4 isoforms, ChemMedChem 7 (2012) 1202–1209, http://dx.doi.org/10.1002/cmdc.201200160.
[4] A.D. Becke, Density-functional exchange-energy approximation with correct asymptotic-behavior, Phys. Rev. A 38 (1988) 3098–3100.
[5] C. Lee, W. Yang, R.G. Parr, Development of the Colle–Salvetti correlation-energy formula into a functional of the electron-density, Phys. Rev. B 37 (1988) 785–789.
[6] A.D. Becke, Density-functional thermochemistry. III. The role of exact exchange, J. Chem. Phys. 98 (1993) 5648–5652.
[7] S. Shaik, D. Kumar, S.P. de Visser, A. Altun, W. Thiel, Theoretical perspective on the structure and mechanism of cytochrome P450 enzymes, Chem. Rev. 105 (2005) 2279–2328, http://dx.doi.org/10.1021/cr030722j.
[8] S. Shaik, S. Cohen, Y. Wang, H. Chen, D. Kumar, W. Thiel, P450 enzymes: their structure, reactivity, and selectivity-modeled by QM/MM calculations, Chem. Rev. 110 (2010) 949–1017, http://dx.doi.org/10.1021/cr900121s.
[9] P. Rydberg, L. Olsen, U. Ryde, Quantum-mechanical studies of reactions performed by cytochrome P450 enzymes, Curr. Inorg. Chem. 2 (2012) 292–315, http://dx.doi.org/10.2174/1877944111202030292.
[10] P. Rydberg, L. Olsen, The accuracy of geometries for iron porphyrin complexes from density functional theory, J. Phys. Chem. A 113 (2009) 11949–11953, http://dx.doi.org/10.1021/jp9035716.
[11] M.-S. Liao, J.D. Watts, M.-J. Huang, Assessment of the performance of density-functional methods for calculations on iron porphyrins and related compounds, J. Comput. Chem. 27 (2006) 1577–1592, http://dx.doi.org/10.1002/jcc.20458.
[12] N. Strickland, J.N. Harvey, Spin-forbidden ligand binding to the ferrous-heme group: ab initio and DFT studies, J. Phys. Chem. B 111 (2007) 841–852, http://dx.doi.org/10.1021/jp064091j.
[13] M.D. Wodrich, C. Corminboeuf, P. von Ragué Schleyer, Systematic errors in computed alkane energies using B3LYP and other popular DFT functionals, Org. Lett. 8 (2006) 3631–3634, http://dx.doi.org/10.1021/ol061016i.
[14] J. Tirado-Rives, W.L. Jorgensen, Performance of B3LYP density functional methods for a large set of organic molecules, J. Chem. Theory Comput. 4 (2008) 297–306, http://dx.doi.org/10.1021/ct700248k.
[15] B.J. Lynch, D.G. Truhlar, How well can hybrid density functional methods predict transition state geometries and barrier heights? J. Phys. Chem. A 105 (2001) 2936–2941, http://dx.doi.org/10.1021/jp004262z.
[16] M. Hall, D. Goldfeld, Localized orbital corrections for the barrier heights in density functional theory, J. Chem. Theory Comput. 5 (2009) 2996–3009, http://dx.doi.org/10.1021/ct9003965.
[17] M. Hall, J. Zhang, Continuous localized orbital corrections to density functional theory: B3LYP-CLOC, J. Chem. Theory Comput. 6 (2010) 3647–3663, http://dx.doi.org/10.1021/ct100418n.
[18] T.F. Hughes, J.N. Harvey, R.A. Friesner, A B3LYP-DBLOC empirical correction scheme for ligand removal enthalpies of transition metal complexes: parameterization against experimental and CCSD(T)-F12 heats of formation, Phys. Chem. Chem. Phys. 14 (2012) 7724–7738, http://dx.doi.org/10.1039/c2cp40220c.
[19] R. Lonsdale, J.N. Harvey, A.J. Mulholland, Compound I reactivity defines alkene oxidation selectivity in cytochrome P450cam, J. Phys. Chem. B 114 (2010) 1156–1162, http://dx.doi.org/10.1021/jp910127j.
[20] R. Lonsdale, J.N. Harvey, A.J. Mulholland, Inclusion of dispersion effects significantly improves accuracy of calculated reaction barriers for cytochrome P450 catalyzed reactions, J. Phys. Chem. Lett. 1 (2010) 3232–3237, http://dx.doi.org/10.1021/jz101279n.
[21] R. Lonsdale, J.N. Harvey, A.J. Mulholland, Effects of dispersion in density functional based quantum mechanical/molecular mechanical calculations on cytochrome P450 catalyzed reactions, J. Chem. Theory Comput. 8 (2012) 4637–4645, http://dx.doi.org/10.1021/ct300329h.
[22] S. Grimme, J. Antony, S. Ehrlich, H. Krieg, A consistent and accurate ab initio parametrization of density functional dispersion correction (DFT-D) for the 94 elements H-Pu, J. Chem. Phys. 132 (2010) 154104, http://dx.doi.org/10.1063/1.3382344.
[23] R. Ahlrichs, M. Bar, M. Haser, H. Horn, C. Kolmel, Electronic-structure calculations on workstation computers – the program system turbomole, Chem. Phys. Lett. 162 (1989) 165–169.
[24] S.H. Vosko, L. Wilk, M. Nusair, Accurate spin-dependent electron liquid correlation energies for local spin density calculations: a critical analysis, Can. J. Phys. 58 (1980) 1200–1211, http://dx.doi.org/10.1139/p80-159.
[25] A. Schafer, H. Horn, R. Ahlrichs, Fully optimized contracted Gaussian-basis sets for atoms Li to Kr, J. Chem. Phys. 97 (1992) 2571–2577.
[26] W.J. Hehre, R. Ditchfield, J.A. Pople, Self-consistent molecular-orbital methods. XII. Further extensions of Gaussian-type basis sets for use in molecular-orbital studies of organic-molecules, J. Chem. Phys. 56 (1972) 2257–2261.
[27] P. Hariharan, J. Pople, The influence of polarization functions on molecular orbital hydrogenation energies, Theor. Chim. Acta 28 (1973) 213–222.
[28] M.M. Francl, W.J. Pietro, W.J. Hehre, J.S. Binkley, M.S. Gordon, D.J. Defrees, et al., Self-consistent molecular orbital methods. XXIII. A polarization-type basis set for second-row elements, J. Chem. Phys. 77 (1982) 3654–3665.
[29] L. Rulísek, K.P. Jensen, K. Lundgren, U. Ryde, The reaction mechanism of iron and manganese superoxide dismutases studied by theoretical calculations, J. Comput. Chem. 27 (2006) 1398–1414, http://dx.doi.org/10.1002/jcc.20450.
[30] R. Krishnan, J.S. Binkley, R. Seeger, J.A. Pople, Self-consistent molecular-orbital methods. XX. Basis set for correlated wave-functions, J. Chem. Phys. 72 (1980) 650–654.
[31] A.D. Mclean, G.S. Chandler, Contracted Gaussian-basis sets for molecular calculations. I. Second row atoms, $Z = 11–18$, J. Chem. Phys. 72 (1980) 5639–5648.
[32] P. Rydberg, P. Vasanthanathan, C. Oostenbrink, L. Olsen, Fast prediction of cytochrome P450 mediated drug metabolism, ChemMedChem 4 (2009) 2070–2079, http://dx.doi.org/10.1002/cmdc.200900363.
[33] P.J.J. Hay, W.R.W.R. Wadt, Ab initio effective core potentials for molecular calculations. Potentials for K to Au including the outermost core orbitals, J. Chem. Phys. 82 (1985) 299–310.
[34] M. Dolg, U. Wedig, H. Stoll, H. Preuss, Energy-adjusted ab initio pseudopotentials for the first row transition elements, J. Chem. Phys. 86 (1987) 866, http://dx.doi.org/10.1063/1.452288.
[35] S. Grimme, Accurate description of van der Waals complexes by density functional theory including empirical corrections, J. Comput. Chem. 25 (2004) 1463–1473, http://dx.doi.org/10.1002/jcc.20078.
[36] S. Grimme, Semiempirical GGA-type density functional constructed with a long-range dispersion correction, J. Comput. Chem. 27 (2006) 1787–1799, http://dx.doi.org/10.1002/jcc.20495.
[37] R.J. Krause, A.A. Elfarra, Oxidation of butadiene monoxide to meso- and (±)-diepoxybutane by cDNA-expressed human cytochrome P450s and by mouse, rat, and human liver microsomes: evidence for preferential hydration of meso-diepoxybutane in rat and human liver microsomes, Arch. Biochem. Biophys. 337 (1997) 176–184, http://dx.doi.org/10.1006/abbi.1996.9781.
[38] M. Kot, W.A. Daniel, The relative contribution of human cytochrome P450 isoforms to the four caffeine oxidation pathways: an in vitro comparative study with cDNA-expressed P450s including CYP2C isoforms, Biochem. Pharmacol. 76 (2008) 543–551, http://dx.doi.org/10.1016/j.bcp.2008.05.025.
[39] H.R. Ha, J. Chen, S. Krahenbuhl, F. Follath, Biotransformation of caffeine by cDNA-expressed human cytochromes P-450, Eur. J. Clin. Pharmacol. 49 (1996) 309–315.
[40] R.E. White, J.T. Groves, G.A. McClusky, Electronic and steric factors in regioselective hydroxylation catalyzed by purified cytochrome P-450, Acta Biol. Med. Ger. 38 (1979) 475–482.
[41] A.D.N. Vaz, D.F. McGinnity, M.J. Coon, Epoxidation of olefins by cytochrome P450: evidence from site-specific mutagenesis for hydroperoxo-iron as an electrophilic oxidant, Proc. Natl. Acad. Sci. U. S. A. 95 (1998) 3555–3560.
[42] S. Yoshioka, S. Takahashi, K. Ishimori, I. Morishima, Roles of the axial push effect in cytochrome P450cam studied with the site-directed mutagenesis at the heme proximal site, J. Inorg. Biochem. 81 (2000) 141–151.
[43] J.T. Groves, G.E. Avaria-Neisser, K.M. Fish, M. Imachi, R.L. Kuczkowski, Hydrogen-deuterium exchange during propylene epoxidation by cytochrome P-450, J. Am. Chem. Soc. 108 (1986) 3837–3838, http://dx.doi.org/10.1021/ja00273a053.
[44] R.A. Mirghani, U. Yasar, T. Zheng, J.M. Cook, L.L. Gustafsson, G. Tybring, et al., Enzyme kinetics for the formation of 3-hydroxyquinine and three new metabolites of quinine in vitro; 3-hydroxylation by CYP3A4 is indeed the major metabolic pathway, Drug Metab. Dispos. 30 (2002) 1368–1371.
[45] T.L. Nielsen, B.B. Rasmussen, J.P. Flinois, P. Beaune, K. Brosen, In vitro metabolism of quinidine: the (3S)-3-hydroxylation of quinidine is a specific marker reaction for cytochrome P-4503A4 activity in human liver microsomes, J. Pharmacol. Exp. Ther. 289 (1999) 31–37.
[46] R.P. Gupta, Y.A. He, K.S. Patrick, J.R. Halpert, N.H. Bell, CYP3A4 is a vitamin D-24- and 25-hydroxylase: analysis of structure function by site-directed mutagenesis, J. Clin. Endocrinol. Metab. 90 (2005) 1210–1219, http://dx.doi.org/10.1210/jc.2004-0966.
[47] X. Zhang, Homolytic bond dissociation enthalpies of the C—H bonds adjacent to radical centers, J. Org. Chem. 63 (1998) 1872–1877, http://dx.doi.org/10.1021/jo971768d.
[48] P.E.M. Siegbahn, F. Himo, The quantum chemical cluster approach for modeling enzyme reactions, WIREs Comput. Mol. Sci. 1 (2011) 323–336, http://dx.doi.org/10.1002/wcms.13.
[49] M. Ekroos, T. Sjögren, Structural basis for ligand promiscuity in cytochrome P450 3A4, Proc. Natl. Acad. Sci. U. S. A. 103 (2006) 13682–13687, http://dx.doi.org/10.1073/pnas.0603236103.
[50] P. Rydberg, U. Ryde, L. Olsen, Sulfoxide, sulfur, and nitrogen oxidation and dealkylation by cytochrome P450, J. Chem. Theory Comput. 4 (2008) 1369–1377, http://dx.doi.org/10.1021/ct800101v.
[51] T.F. Hughes, R.A. Friesner, Development of accurate DFT methods for computing redox potentials of transition metal complexes: results for model complexes and application to cytochrome P450, J. Chem. Theory Comput. 8 (2012) 442–459, http://dx.doi.org/10.1021/ct2006693.